Imaging *S*-wave scatterer distribution in southeast part of the focal area of the 2005 West Off Fukuoka Prefecture Earthquake (M_{JMA}7.0) by dense seismic array

Satoshi Matsumoto[1], Atsushi Watanabe[1], Takeshi Matsushima[1], Hiroki Miyamachi[2], and Syuichiro Hirano[2]

[1]*Institute of Seismology and Volcanology, Faculty of Sciences, Kyushu University, Shimabara, Japan*
[2]*Faculty of Science, Kagoshima University, Kagoshima, Japan*

(Received August 19, 2005; Revised February 3, 2006; Accepted February 14, 2006; Online published February 2, 2007)

Spatial distribution of *S*-wave scatterers in the SE part of the focal area of the 2005 West Off Fukuoka Prefecture Earthquake ($M = 7.0$) has been estimated using dense seismic array data. Waveforms of 22 natural earthquakes were analyzed in a frequency range of 16–24 Hz. It is difficult to estimate the inhomogeneous structure in this wavelength range with ordinary travel time tomography despite the importance of this parameter for understanding the earthquake-generating process. After filtering and gain recovery in the coda part, observed waveforms were semblance-enhanced slant-stacked into various directions from the array. This was followed by diffraction curve summation in order to image the scatterer distribution. The spatial distribution of scatterers thus imaged revealed that higher strengths were distributed at the SE-extension of the fault plane of the event, which corresponds to a region where the rupture process of the main shock stopped.

Key words: Scatterer, seismic array, 2005 West off Fukuoka Prefecture earthquake.

1. Introduction

In general, many phases appear in the seismogram of natural earthquakes and artificial explosions following the arrival of direct *P*- and *S*-waves. Nishigami (1991, 2000) and Revenaugh (1995) estimated scatterer distribution and discussed the relationship between inhomogeneity and seismicity based on an analysis of regional seismic network data. Observations on the seismic array can detect small-scale structures because the directional sensitivity of the array can be tuned to a target direction. If we analyze seismograms recorded by a small aperture array with stations several tens of meters apart, the ray direction approaching the array could be determined in more detail. Matsumoto *et al*. (1998) imaged the scatterer distribution around the focal area of the 1995 Kobe earthquake from the slant-stacked waveform obtained by a small aperture array. Seismic array analysis is one of the best approaches to obtain precise information on the inhomogeneity of the Earth's interior.

The West Off Fukuoka Prefecture Earthquake occurred on March 20, 2005 with a magnitude on the JMA scale of 7.0. The main shock fault and most of the epicenters of the aftershocks were located in the Genkai Nada Sea, situated at the southeastern end of the Japan Sea. The type of faulting for this earthquake is left-lateral strike slip. Based on the aftershock distribution, the faulting of the main shock appears to have stopped beneath Shikanoshima Island. The features of this earthquake were described in detail by Shimizu *et al*. (2006); consequently, we limit ourselves in this study to an estimation of scatterer distribution around the focal area using dense seismic array data and discuss the characteristics of the earthquake from the perspective of an inhomogeneous structure.

2. Observation and Data

In order to detect scattered waves generated by inhomogeneities in the target area, we carried out observations of natural earthquakes using a seismic array at a monitoring station situated in Nishi Koen Park, which is located in the northern part of Fukuoka City, from April 26 to July 21, 2005. The location of the array was the southeastern extension of the aftershock area of the earthquake, as shown in Fig. 1, in the vicinity of the Kego fault, one of Japan's active faults. The array was composed of 2-Hz horizontal component seismometers and three-component seismometers with a site spacing of 20 m. Three-component seismometers were installed at three sites. The sensor at the one-component station was oriented in a direction parallel to the strike of the Kego fault. In total, there were 66 observation sites for this array. In the present observation, seismometers were distributed two-dimensionally in order to detect scattered waves coming from various directions. Seismic signals were collected through CDP cables and recorded by two digital recorders. The recorders having 24 and 48 channels were equipped with sigma-delta A/D converters with a 24-bit resolution. The recording time for each event was set to 30 s, with a sampling frequency of 500 Hz. Earthquakes were detected automatically by taking ratios of short-term to long-term averaged amplitudes at several sites.

We analyzed waveform data from 18 earthquakes whose

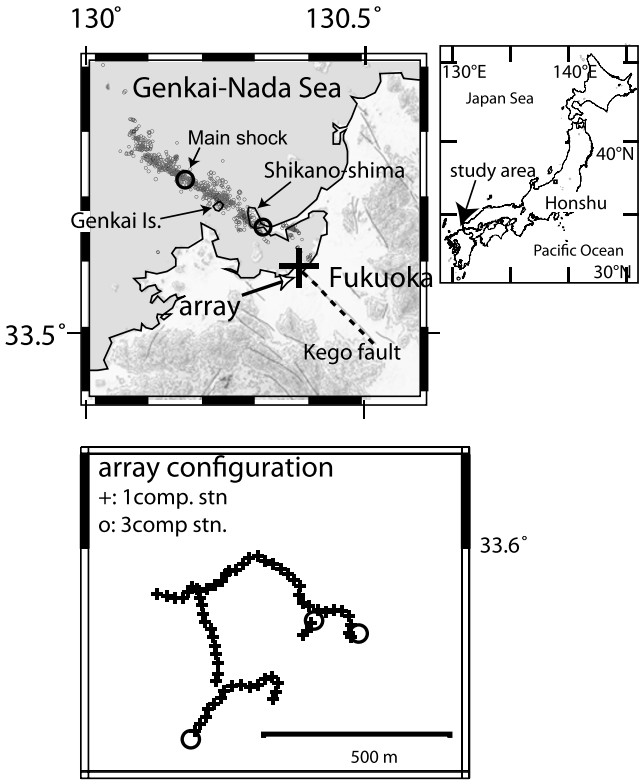

Fig. 1. Map showing the locations of a seismic array and the main and aftershock distribution of the 2005 West Off Fukuoka Prefecture Earthquake, as determined by Uehira *et al*. (2006). Large circles show the main shock and largest aftershock of the earthquake. Small circles denote other aftershocks. A cross denotes the array location. The seismic array configuration is displayed in the lower figure. Crosses and circles in the lower figure denote the locations of observation sites of the array.

locations are shown in Fig. 4. The selected earthquakes had a magnitude greater than 2 and made a positive contribution to improving the imaging of the scatterer distribution based on the resolution check described in the following section. The hypocenters were located by using data obtained from a temporal seismic network (Uehira *et al*., 2006). The uncertainty of the hypocenter locations averaged 0.5 km horizontally and 1 km vertically. An example of a record section for the event that occurred on May 5, 2005, the largest event among the ones triggered during the observation period, is shown in Fig. 2. In this figure, the waveform data are band-pass filtered in the frequency range 16–24 Hz, with a decay of −12db/Oct., and the coda part is amplified by auto gain control processing with a time window of 4 s. In Fig. 2, several phases are clearly visible in the coda part following direct S-wave onset. These phases can be identified in the recording section even without the amplitude recovery procedure. In the following section, an array analysis is applied to these data to estimate the detailed spatial distribution of scatterers.

3. Analysis

Ray directions of scattered waves can be expressed as a function of slowness and azimuth from the array, and the scatterer location can be determined from the ray direction of the scattered wave and from its travel time. The procedure of stacking traces from event to event reveals the scatterer distribution at a high resolution. However, the events analyzed here are natural earthquakes. In such cases, we cannot apply high-resolution analyses developed in exploration seismology, such as CDP stacking and migration processing, due to the characteristics of natural earthquakes, including the effect of the radiation pattern from the seismic source. This pattern complicates the polarity of ground motion at a station. Not all scattered waves from a scatterer interfere constructively at the station since the polarity of the scattered wave depends on both the emergent direction from the source to the scatterer and the source mechanism. In this study, we adopt a processing sequence to estimate the spatial distribution of scatterers as follows.

The sequence basically follows Matsumoto *et al*. (1998) using slant stack processing. The flow chart of the sequence is shown in Fig. 3. A slant-stacked waveform of a certain azimuth and slowness can be regarded as scattered waves coming from that direction along the ray path with that slowness. In this process, waveform data in the space-time domain are converted to the slowness, azimuth-time domain. Several procedures are applied to the data prior to stacking. First, station corrections at every site are estimated to remove the travel time anomaly between stations, which is mainly caused by the inhomogeneous velocity structure near the surface where the sensors are installed. For each event, the time difference at each site is defined as the residual of the manually picked arrival time of the direct S-wave to the calculated one. The optimum plane wave front of the direct S-wave is estimated from the manually picked time by least squares fitting, thereby providing the calculated arrival times for every station. By taking an average of the time differences for all events, we obtain the static correction factor at each site. We assume here that scattered waves approach the array as plane waves. Curvature of the wave front of these scattered waves affects the amplitude of the slant-stacked waveform if the time difference between the spherical wave front and plane wave front at the edge of the array is greater than a quarter period for the target frequency. Therefore, we will discuss scatterers located 1 km or more away from the array.

The waveform for each pair of events and stations is passed through a band-pass filter and subjected to gain recovery processing. The pass-band of the filter is from 16 to 24 Hz. Before gain recovery, a muting process for the direct S-wave is applied in order to avoid contaminating the image of the scatterer distribution with a direct S-wave having a large amplitude. As the gain recovery process, we fit an exponential function to the root-mean-square amplitude of the waveform-corrected geometrical factor defined in the single scattering model (Sato and Fehler, 1997), and calculate the residual between the function and the observed waveform. The amplitude recovery corresponds to normalizations for source energy and for scattered energy by uniformly distributed scatterers.

In this study, we adopt "semblance-enhanced slant stacking" as the stacking procedure. The ordinary slant stacking used in Matsumoto *et al*. (1998) is one of the classical beam-forming techniques used in array signal processing. Because of the accuracy of estimation and the

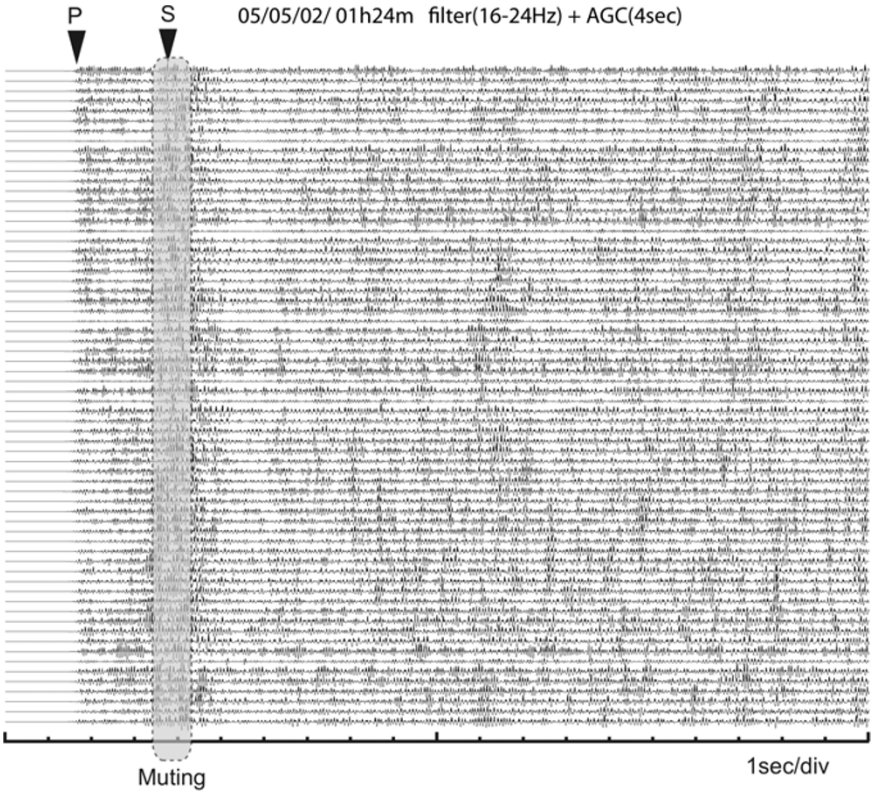

Fig. 2. An example of a seismic section recorded by the seismic array. A bandpass filter of 16–24 Hz and AGC processing were applied.

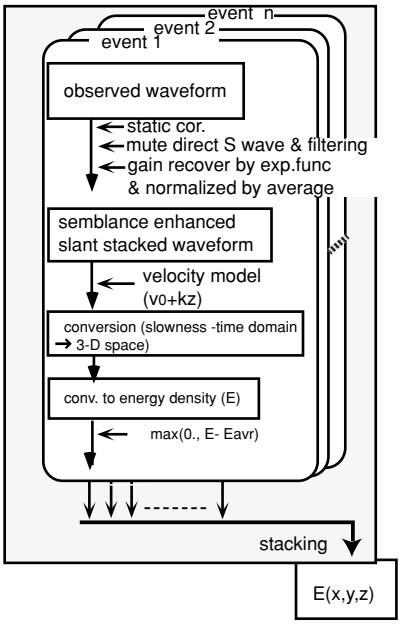

Fig. 3. Flowchart of the processing used in this study.

small number of calculations required, slant-stack processing is basically used in this study. Matsumoto *et al.* (2002) also estimated detailed scatterer distribution in the hypocentral area of the 2000 Western Tottori Earthquake using semblance-enhanced slant stacking. The semblance-enhanced slant stack makes it very simple to process observed data. The output signal at the lapse time using this processing approach is obtained from the slant-stacked waveform weighted by the semblance coefficient. The coefficient relating to the cross-correlation between waveforms is calculated from the waveform data within a time window around the lapse time. In the present study, the time window is set at 0.4 s. The semblance coefficient for the slowness vector $\vec{s}$ for the waveforms $d(t)$ observed by an array can be calculated by the following formula (Neidell and Taner, 1971);

$$S(t,\vec{s}) = \frac{\sum_{j=1}^{M}\left[\sum_{i=1}^{N} d_i(t_j - \vec{s}\cdot\vec{x}_i)\right]^2}{N\sum_{j=1}^{M}\sum_{i=1}^{N} d_i(t_j - \vec{s}\cdot\vec{x}_i)^2}$$

where M and N are the number of data points within a time window and the number of stations for stacking, respectively. $\vec{x}$ is the positioning vector of a site composing the array. The observed waveforms are stacked in terms of variable slowness, with the north-south and east-west components of the slowness vector used here ranging from -0.33 to 0.33 with a step interval of 0.01. Semblance-enhanced stacking is a high-resolution technique despite the simplicity of the calculation. Although resolution is improved by the enhancement, amplitude is not always precise as scattered wave strength is used to estimate the scattering coefficient.

After the stacking, the waveform is transformed into the horizontal distance azimuth-depth domain from the time-slowness domain based on the S-wave velocity structure. A scatterer location can be calculated from slowness, lapse time, and the locations of the hypocenter and array. Here, we adopt a depth-dependent velocity model expressed by

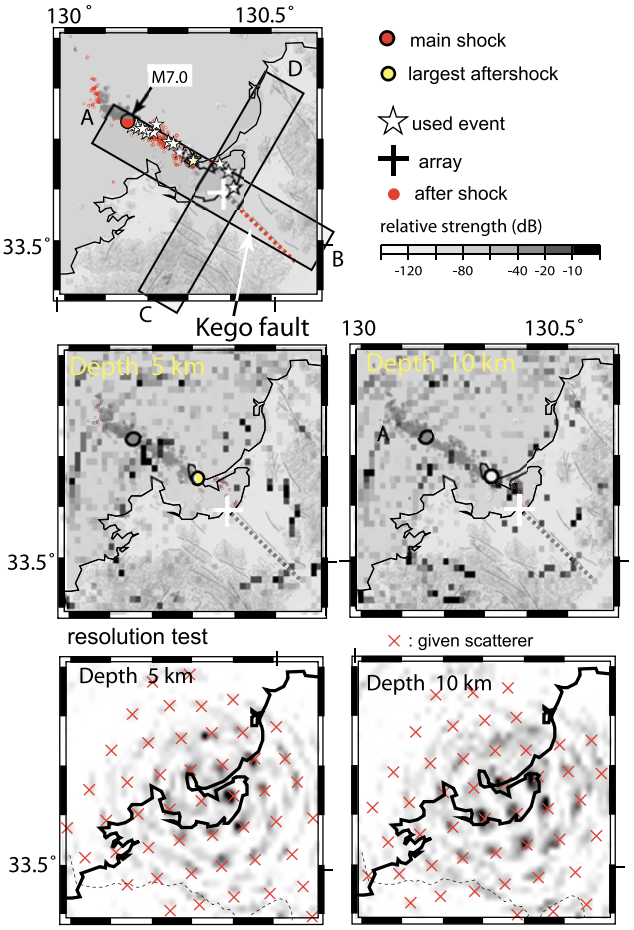

Fig. 4. Map of the obtained scatterer distribution (middle) and the results of the resolution check (bottom) at depths of 5 and 10 km. The gray scale shows the relative strength of scattering. Open star in the top figure indicates the epicenter analyzed. Other symbols are the same as those in Fig. 1. Rectangular areas labeled A–B and C–D show the horizontal locations of vertical cross-sections in Fig. 5. In the upper and middle figures, the topography in this area is also shown. The green color indicates a relatively high altitude. Red crosses in the bottom figure show the scatterer locations given in the resolution check.

$v(z) = v_0 + kz$, where z is depth in kilometers, and v_0 and k are 3.06 km/s and 0.033 1/s, respectively. This velocity structure is obtained by smoothing the model adopted by Shimizu *et al.* (2006) to determine the hypocenters in this region. We also assume that multiple-scattered waves can be ignored. Treating data from one event with this process gives a spatial distribution of relative scattering strength for an S-wave.

We stacked all of the waveforms obtained from the 18 events to improve the image of the relative scattering strength distribution. Although the time interval of each sample in slant-stacked waveforms of events with a certain slowness is identical with each other, which is the inverse of the sampling frequency of an A/D converter, the distance interval corresponding to each time sample varies from event to event. In particular, the sample interval of slant-stacked waveforms expands in smaller lapse times. This means that waveform shape is deformed by the processing. This effect depends on the offset distance between the array and the source. Both this factor and the polarity uncertainty described earlier due to the radiation pattern of the earthquake do not allow the processed waveforms of all the events to be stacked in order to improve the S/N ratio. Therefore, we deal with the processed waveforms as an energy density series by considering the power of the stacked waveform. The energy density with a uniform distance interval is obtained from an interpolation of those with a varying distance interval. We can then stack them for all the events, which provides an image of the spatial distribution of the relative scattering strength for the S-wave. In the present study, scattering strength is evaluated by energy density stacking. Background scattered energy clouds the image of a stronger scatterer distribution as the number of stacks increases. Therefore, we subtract the average density of each energy density sequence from the original energy sequence before stacking. For the homogeneous velocity model, Sato (1977) analytically obtained the result that the energy density of the coda wave is in proportion to the scattering coefficient (g_0) based on the single isotropic scattering assumption. Therefore, the ratio of energy density to the smoothed coda energy envelope at a lapse time is equal to that of scattering coefficient (g) to background scattering coefficient (g_0) in terms of the volume contributing to coda energy at that lapse time. In our analysis, the process of taking the ratio corresponds to a gain recovery process. For the depth-dependent velocity structure, it can be considered that the ratio is still g/g_0. However, this interpretation can also be made for the ordinary slant stack procedure. The image created by the processing method used in this study is weighted one by its relative confidence and the semblance value becomes one for completely correlated scattered phases among sites. In such a case, the image corresponds to the distribution of g/g_0. However, a scattered phase contaminated by scattered phases from other directions could not provide a semblance value of one. This implies that the semblance value reflects the reliability of the stacked amplitude. We then interpret that the result finally obtained is the ratio $(g - g_0)/g_0$ because of applying the gain recovery and subtracting the average value.

The processing described above is essentially identical to the diffraction curve summation of the energy density sequence among events. To check the resolution of this method, we synthesize scattered waves from point-scatterers located beneath the array for 18 events. The scatterers are uniformly distributed at intervals 10 km apart horizontally and 5 km deep. The processing described above is applied to the synthesized waveform. After stacking the energy density sequences for all the events, we can accurately calculate the given scatterer distribution within a distance of less than 20 km from the array. The results are shown in Figs. 4 and 5 together with the scatterer distribution estimated using actual data. The estimation error is less than a few kilometers in the shallower part, as can be seen in Figs. 4 and 5.

4. *S*-wave Scatterer Distribution

Images obtained by stacking for the 18 events are shown in Figs. 4 and 5. These figures show horizontal maps and vertical cross-sections of the relative scattering strength distribution. We display the vertical cross-sections along A–B

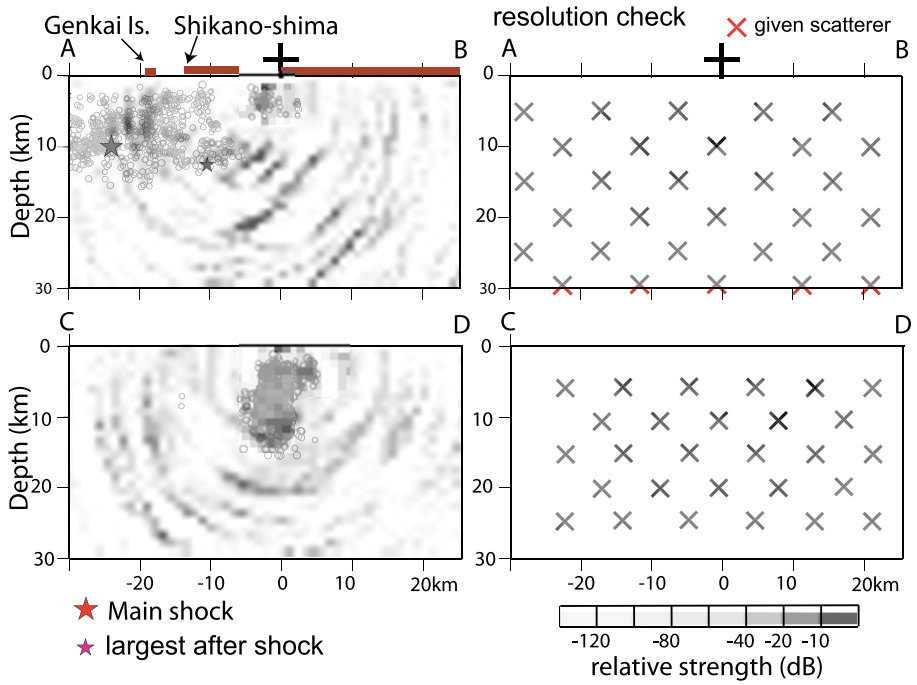

Fig. 5. Vertical cross sections of *S*-wave scatterer distribution (left) and results of the resolution check (right). The cross sections are along line A–B (upper) and line C–D (lower), respectively, shown in Fig. 4. Relative scattering strength is shown by the scale at the bottom. The dark portion shows high scattering strength. The black cross is the location of the array. Red circles show the hypocenters of the aftershock. Large and small red stars in the upper left indicate the main shock and the largest aftershock, respectively. The red cross to the left shows the scatterer location given in the resolution check.

and C–D in Fig. 4 after obtaining averages of the scattering strengths along the shorter leg of the rectangle. These are parallel and perpendicular to the fault plane of the main shock. Some areas having a relatively high scattering strength are clearly visible in Fig. 4. Strong scatterers exist to the south and east of the array at a depth of 5 km, and this can be also found around Genkai Island where the strongest ground motion accompanying the main shock faulting was observed. The strong scatterers located in the south of the array are still seen in the deeper sections. At 10 km, we can identify a strong part beneath the bay adjacent to the array; this feature can be seen in the vertical cross section (Fig. 5). The dark portion corresponds to the strong scatterers that are mainly distributed in the southeastern part of the aftershock area; these are clustered at depths of about 10 and 22 km at the southeastern extension of the aftershock area. In cross section C–D, high-strength scatterers are also distributed at depths of 6–10 km that correspond to those scatterers located in the south and east part of Fig. 4. There are few high-strength scatterers in the region further than 25 km from the array, mainly due to the detectability of the array using the data set of the present study as the detectability of the scatterer distribution obtained from events at long distances becomes low in the region containing both of the event and the array locations. In addition, the earthquakes used here were distributed only in the northwest and, as such, the detection capability is lower in the northwestern part of the target region.

The strong scatterers at a depth of 5 km are distributed in the south and east regions, corresponding to a mountainous region that was formed in the Paleozoic and is characterized by the presence of intruded granitic rocks (Geological Survey of Japan, 1993). Most of the mountain regions are covered by granitic rocks and, in general, the inhomogeneities caused by the granitic intrusions continue into a deeper part of the crust. Therefore, the scatterers could reflect this inhomogeneity. The strong scatterers exist at a depth of about 10 km beneath the array, as seen in the vertical cross section (Fig. 5). The southeastern part of the region has stronger inhomogeneity than the northwestern part. The red circles displayed in Fig. 5 are hypocenters of the aftershock of the 2005 West Off Fukuoka Prefecture Earthquake. The aftershock distribution suggests that the rupture of the main shock stopped beneath Shikanoshima Island, which may be related to the existence of strong inhomogeneities in the southeast extension of the main shock fault. The largest aftershock occurred at the edge of the main shock fault, adjacent to the strong scatterer. In the target area, there is an active fault, denoted Kego, as shown by the dotted line in Fig. 4. The inhomogeneity directly relating to the Kego fault is not always clearly identified. However, the strong inhomogeneity could be imaged at the northwest extension of the fault.

Acknowledgments. We gratefully acknowledge the participants of the seismic array observation. The authors are grateful to the Research Center for Prediction of Earthquakes and Volcanic Eruptions, Tohoku University for their gracious cooperation. Our thanks are extended to the anonymous reviewers for their many helpful suggestions on this paper. We also thank members of the Institute of Seismology and Volcanology, Kyushu University for valuable discussions and cooperation with the observations.

References

Kubo, K., H. Matsuura, M. Ozaki, H. Makimoto, H. Hoshizumi, and K.

Kamada, Geological Survey of Japan, Geolgical Map of Japan 1:200000 Fukuoka, 1993 (in Japanese).

Matsumoto, S. and K. Obara, Imaging P-wave scatter distribution in the focal area of the 1995 M7.2 Hyogo-Ken Nanbu (Kobe) earthquake, *Geophys. Res. Lett.*, **25**, 1439–1442, 1998.

Matsumoto, S., K. Obara, N. Kimura, and M. Nakamura, Imaging P-wave scatterer distribution around the focal area of the 2000 Western Tottori Earthquake (Mw6.6), *Zisin*, **2**, 55, 229–232, 2002 (in Japanese).

Neidell, N. S. and M. T. Taner, Semblance and other coherency measures for multi-channel data, *Geophysics*, **36**, 482–497, 1971.

Nishigami, K., A new inversion method of coda waveforms to determine spatial distribution of coda scatterers in the crust and uppermost mantle, *Geophys. Res. Lett.*, **18**(12), 2225–2228, 1991.

Nishigami, K., Deep crustal inhomogeneity along and around the San Andreas fault system in central California and its relation to the segmentation, *J. Geophys. Res.*, **105**, 7983–7998, 2000.

Revenaugh, J., A scattered-wave image of subduction beneath the transverse range, *Science*, **268**, 1888–1892, 1995.

Sato, H. and M. Fehler, *Seismic Wave Propagation and Scattering in the Heterogeneous Earth*, pp. 1–308, Springer, 1998.

Shimizu, H., H. Takahashi, T. Okada, T. Kanazawa, Y. Iio, H. Miyamachi, T. Matsushima, M. Ichiyanagi, N. Uchida, T. Iwasaki, H. Katao, K. Goto, S. Matsumoto, N. Hirata, S. Nakao, K. Uehira, M. Shinohara, H. Yakiwara, N. Kame, T. Urabe, N. Matsuwo, T. Yamada, A. Watanabe, K. Nakahigashi, B. Enescu, K. Uchida, S. Hashimoto, S. Hirano, T. Yagi, Y. Kohno, T. Ueno, M. Saito, and M. Hori, Aftershock seismicity and fault structure of the 2005 West Off Fukuoka Prefecture Earthquake (M_{JMA}7.0) derived from urgent joint observations, *Earth Planets Space*, **58**, this issue, 1599–1604, 2006.

Uehira, K. ,T. Yamada, M. Shinohara, K. Nakahigashi, H. Miyamachi, Y. Iio, T. Okada, H. Takahashi, N. Matsuwo, K. Uchida, T. Kanazawa, and H. Shimizu, Precise aftershock distribution of the 2005 West Off Fukuoka Prefecture Earthquake (Mj=7.0) using a dense onshore and offshore seismic network, *Earth Planets and Space*, **58**, this issue, 1605–1610, 2006.

S. Matsumoto (e-mail: matumoto@sevo.kyushu-u.ac.jp), A. Watanabe, T. Matsushima, H. Miyamachi, and S. Hirano